ChemComm

COMMUNICATION

View Article Online
View Journal | View Issue

Cite this: *Chem. Commun.*, 2022, **58**, 1784

Received 6th November 2021,
Accepted 6th January 2022

DOI: 10.1039/d1cc06265d

rsc.li/chemcomm

Toroidal *versus* centripetal arrangement of the magnetic moment in a Dy_4 tetrahedron†

Qianqian Yang,[ab] Liviu Ungur, *[c] Liviu F. Chibotaru[d] and Jinkui Tang *[ab]

Magnetic investigation and *ab initio* calculations reveal toroidal arrangement of the magnetic moment rather than centripetal anisotropies in a tetrahedral Dy_4 complex.

Lanthanide complexes have witnessed a renaissance in molecular magnet research in the last two decades due to the highly anisotropic nature that makes them the best candidate for potential applications in high-density information storage and quantum computation devices.[1] In particular, experimental and theoretical chemists have paved the way for how to obtain robust SMMs with high blocking temperature and energy barriers. On one hand, a short ligand contact from an axial direction is necessary to ensure the high anisotropy of lanthanide ions.[2] On the other hand, a specific coordination symmetry, such as D_{4d},[3] D_{5h},[4] and ideal $C_{\infty v}$[5] for the Dy^{III} ion, should be constructed to minimize the quantum tunneling of the magnetization (QTM).[6] These two factors seem to be the wind vane for predicting the SMM property of mononuclear lanthanide complexes. Meanwhile, for polynuclear systems, the low molecular symmetry and various structural topologies make it difficult to give a universal certificate for manipulating the coordination geometry.[7] The preponderant binding of the Ln^{III} ion to one of the ligand atoms sometimes defines the axial crystal field and anisotropy,[2b] which is essential for the design of polynuclear SMMs.[8]

Among polynuclear lanthanide SMMs, there is a special group of molecules, namely single-molecule toroics (SMTs),[9] in which the magnetic moments of spin carriers are in a vortex arrangement, resulting in the bi-stable diamagnetic ground state.[10] The main character of STMs is the toroidal magnetic moment, in other words, the toroidal arranged anisotropy axes. The criterion for polynuclear SMMs seems also to fit for STMs, which only need to restraint the preponderant binding atoms in-plane and bridge the Dy^{III} ions in a circle topology. For instance, in the typical Dy_3 triangle STM, the Dy^{III} ions are bridged by strong μ_2–O donors that induce axial anisotropy on the Dy^{III} ion with anisotropy axes close to the O–Dy–O direction.[11] The subsequently reported Dy_4 square,[12] and Dy_6 circle-based SMTs[13] also show a similar tendency. Additionally, *ab initio* calculations[11a] and single-crystal torque magnetometry studies[14] provide a deep understanding of toroidal magnetic moment behaviors.

Besides the planar arranged dysprosium complexes that behave as SMTs, a Dy_4 cube also shows a typical diamagnetic ground state, in which the magnetic moments are in a 3D net arrangement.[15] As a basic building block, the Dy_4 tetrahedron has great potential for constructing 3D topologies,[16] and could also arrange the magnetic moments in a toroidal way. However, the strong central μ_4–O^{2-} donor usually has a short ligand contact with the lanthanide ions,[17] inducing centripetal anisotropies of the lanthanide ions.

Herein, we reported a **Dy_4** tetrahedral complex where the Dy^{III} ions are in a distorted D_{4d} coordinate geometry. A μ_4–O, as a strong donor, resides in the center of the molecule and bridges the Dy^{III} ions with short contacts. According to the preponderant bond approach, the magnetic anisotropy axes of each Dy^{III} ion probably point to the μ_4–O center and lead to a diamagnetic ground state (Scheme 1). While *ab initio* calculations (*wide infra*) indicate that the anisotropy axes of Dy^{III} ions are not pointing to the μ_4–O donor but along the μ_2–O plane, resulting in SMT behavior in the **Dy_4** tetrahedral topology.

The *in situ* reaction of 2-hydrazino benzothiazole and *o*-vanillin with $Dy(NO_3)_3{\cdot}6H_2O$ in methanol in the presence of

[a] *State Key Laboratory of Rare Earth Resource Utilization, Changchun Institute of Applied Chemistry, Chinese Academy of Sciences, Changchun 130022, P. R. China. E-mail: tang@ciac.ac.cn*
[b] *School of Applied Chemistry and Engineering, University of Science and Technology of China, Hefei 230026, P. R. China*
[c] *Department of Chemistry, National University of Singapore, 117543, Singapore. E-mail: chmlu@nus.edu.sg*
[d] *Theory of Nanomaterials Group and Institute of Nanoscale Physics and Chemistry -INPAC, Katholieke Universiteit Leuven, 3001 Leuven, Belgium*

† Electronic supplementary information (ESI) available: Experimental details and additional figures (Tables S1–S8 and Fig. S1–S14). CCDC 2117123. For ESI and crystallographic data in CIF or other electronic format see DOI: 10.1039/d1cc06265d

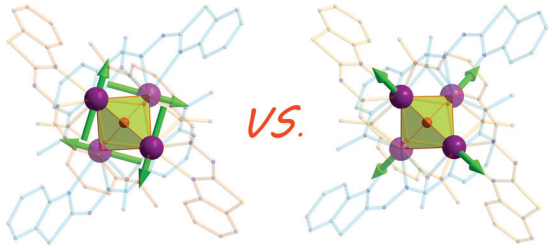

Scheme 1 Schematic drawings of the toroidal (left) and centripetal (right) anisotropy arrangements in the **Dy_4** tetrahedron.

Et_3N produces $[Dy_4(\mu_4\text{–}O)L_2(HL)_2(CH_3O)_4]\cdot 4CH_3OH\cdot H_2O$ (**Dy_4**). Single-crystal X-ray diffraction shows that **Dy_4** crystallizes in the monoclinic *C*2/*c* space group (Table S1, ESI†) and features a neutral tetranuclear structure (Fig. 1). The molecule contains one μ_4–O bridging Dy_4 core, four ligands, four μ_2–O methanol ligands, four methanols, and one water molecule in the lattice. The μ_4–O bridging Dy_4 core resides in the center of the molecule with Dy–O bond distances of 2.18 and 2.19 Å (Table S2, ESI†), and Dy–O–Dy angle ranging from 104.51 to 112.01° (Table S2, ESI†), which is close to the value in a regular tetrahedron (109.28°). Four μ_2–O groups connect the neighboring Dy1 and Dy2 on the edges of the tetrahedron. The ligands, connecting with Dy1 and Dy1′ on the top side are monodeprotonated. The ligands, coordinating with Dy2 and Dy2′ at the bottom side are double-deprotonated (Scheme S1, ESI†), which is related to the relatively longer C–N (in thiazole) bond distances (1.33 Å). The deprotonated and protonated hydrazine groups act as proton acceptors and donors (Fig. S1, ESI†) and contact with the methanol molecules in the lattice by hydrogen bonding, forming 3D hydrogen-bonded frameworks (Fig. S2, ESI†).

Dy^{III} ions are eight coordinated. SHAPE analysis reveals that the Dy^{III} ions are in a distorted square antiprism (D_{4d}) geometry with CShM values of 1.72 and 1.76 for Dy1 and Dy2 (Table S4, ESI†), respectively. The less distortion of the D_{4d} geometry in the molecule probably produces an axial ligand field and strong anisotropy for the Dy^{III} ion. The μ_4–O gives much shorter Dy–O (μ_4–O) bonds ($\leq$ 2.19 Å) than other Dy–O or Dy–N bonds (Table S2, ESI†). While this short bond value gives the impression that the μ_4–O should define the local anisotropy axes on all Dy sites, as shown by an electrostatic approach (Fig. S4 and S5, ESI† for Magellan calculations[18]), the *ab initio* calculations (*wide infra*) show that the joint effect of all the other ligands (of a distorted D_{4d} symmetry) is dominant. This concludes that the crystal field effect of the μ_4–O is divided among four Dy sites and therefore its importance in defining the main anisotropy axis for each Dy^{III} is weaker than expected. Moreover, the Dy···Dy distances in the structure are in the range of 3.45–3.62 Å, which would produce intramolecular magnetic interaction (see below).

DC magnetic measurements reveal that the room temperature $\chi_M T$ product (χ_M = molar magnetic susceptibility) is 55.60 $cm^3\ K\ mol^{-1}$ (Fig. 2), which is in good agreement with the value expected for four free-ion approximation of Dy^{III} ions ($S = 5/2$, $L = 5$, $^6H_{15/2}$, $g = 4/3$). Upon cooling, the $\chi_M T$ products decrease gradually before a quick drop at 20 K and reach the value of 14.77 $cm^3\ K\ mol^{-1}$ at 2 K. The quick drop at low temperatures can be attributed to the dominated antiferromagnetic interaction between the Dy^{III} ions (see the *ab initio* calculation below). The magnetizations *versus* field plots for the complex reveal a quick increase without saturation (Fig. S6, ESI†), indicating the presence of magnetic anisotropy and/or the crystal-field effects. The *M versus. H*/*T* plot at 1.9 K shows a relatively slower increase in the low field region and then

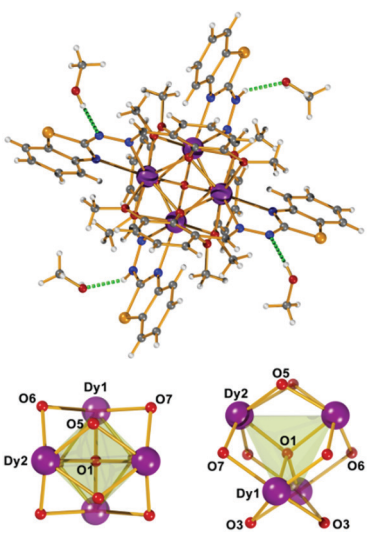

Fig. 1 Structure of **Dy_4**. The purple, blue, grey, white, orange, and red spheres represent Dy, N, C, H, S, and O, respectively. The green dashed lines represent the hydrogen bonds.

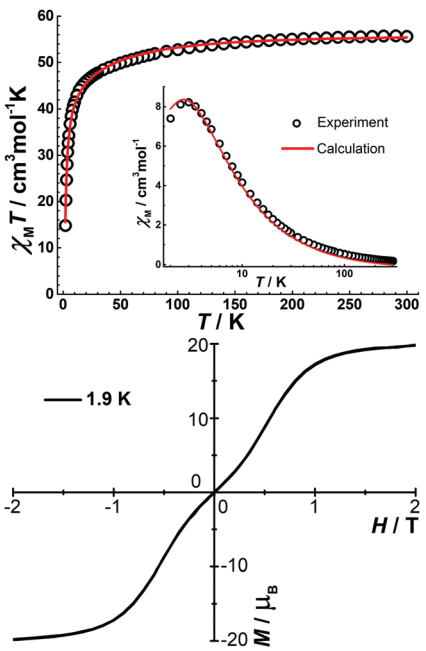

Fig. 2 Temperature-dependent $\chi_M T$ products at 1 kOe (top) and molar magnetization (*M*) *versus H* at 1.9 K (bottom) for **Dy_4**. Inset represents the relevant χ_M *versus T* plot.

increases fast at higher field (Fig. S7, ESI†). This effect is very significant at 1.9 K for the measurement in the range of −2 to 2 T (Fig. 2, bottom). The differential of the molar magnetization shows a minimum at zero field (Fig. S8, ESI†), suggesting the existence of the diamagnetic ground state, which is consistent with the decrease of magnetic susceptibility at low temperatures.

AC measurements were performed to investigate the dynamic magnetic properties. The out-of-phase χ'' signal shows temperature- and frequency-dependency at low temperatures (Fig. 3 and Fig. S9, ESI†). In particular, χ'' peaks are observed under zero dc field, indicating the typical SMM behavior. The Cole–Cole plots represented as χ'' *versus* χ' (Fig. S10, ESI†) reveal semi-circular profiles. Fitting the plots with a generalized Debye model[19] gave α parameters in the range of 0.2–0.41, indicating a broad distribution of relaxation times. Extracting the relaxation times (τ) from the maxima of frequency-dependent χ'' and fitting the relevant τ *versus* $1/T$ by using the following equation:[20]

$$\frac{1}{\tau_{obs}} = CT^n + \tau_0^{-1}\exp\left(-U_{eff}/T\right)$$

where CT^n and $\tau_0 \exp(U_{eff}/T)$ represent Raman and Orbach relaxation processes,[19] respectively, gives the barrier U_{eff} of 1.97 K with $\tau_0 = 2.1 \times 10^{-4}$ s, $C = 1.91$, and $n = 3.76$ (Fig. S11, ESI†).

To gain insight into the magnetic anisotropy, *ab initio* calculations have been performed on **Dy$_4$** based on the X-ray determined structure. Mononuclear Dy^{III} fragments have been included in the calculation of CASSCF/RASSI/SINGLE_ANISO type with the OpenMOLCAS program package,[21] in which all other three Dy^{III} ions were computationally substituted by diamagnetic Lu^{III} ions, while keeping the ligand frame intact. The DZP basis set approximations have been employed on each Dy^{III} ion. As shown in Table S5 (ESI†), the lowest spin–orbit states ($M_J = \pm 15/2$) of each Dy^{III} ion are well separated from the excited states. Within the ground multiplet, the eight doublets

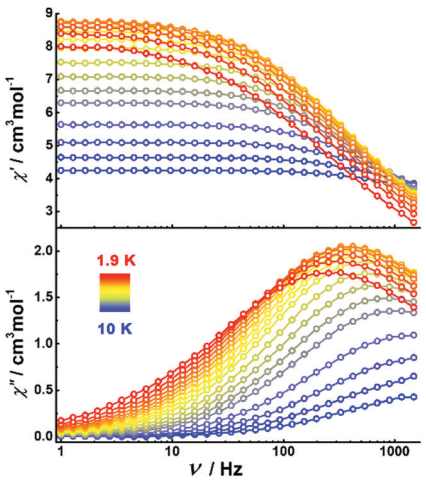

Fig. 3 Frequency dependence of ac susceptibility for **Dy$_4$** at indicated temperatures under zero dc field.

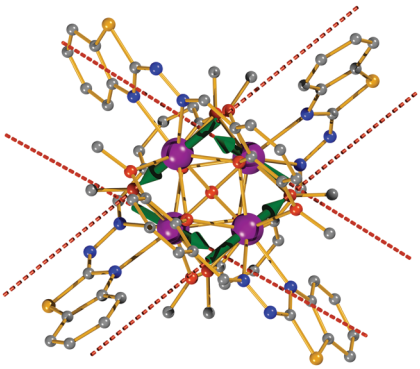

Fig. 4 Orientations of the main magnetic axes and local magnetizations in the ground state of the **Dy$_4$** complex.

show Ising type anisotropy because of the Kramers nature of the Dy^{III} ion. The ground doublet of each Dy^{III} ion features axial anisotropy with a $g_z \gg g_{x,y}$ (Table S5, ESI†). The energy gap between the ground doublet and the first excited state is more than 46.26 cm^{-1} for each Dy^{III} ion. While, due to the still existences of non-ignored transverse components (g_x and g_y) and magnetic couplings (Table S8, ESI†), fast quantum tunneling of magnetization would probably occur at individual Dy^{III} ions and accelerate the relaxation of magnetization. The efficient barrier from the experiment is much smaller than that from the calculation. The main magnetic axes of Dy^{III} ions are determined from the calculation to check the magnetic ground state of the molecule. As shown in Fig. 4, the anisotropy axes are arranged toroidally when viewing along the *b* axis, which is different from what we expected from electrostatic considerations or bond length analysis (Table S7, ESI†). The reason for this effect is that the crystal field effect of the central μ_4–O is divided among all four bonding Dy sites and is effectively smaller than expected if it was bonding one single Dy site. As a result, the anisotropic axes are dominated by the other ligands surrounding each Dy site and by their coordination geometry.[22] This behavior is similar to the net toroidal magnetic moment in a Dy$_4$ cubic complex. The orthogonal arrangement of magnetic moment results in a small resulting magnetic moment in the ground state ($\approx 4.4\ \mu_B$), oriented perpendicular to the plane of the image in Fig. 4, which is in good agreement with the dc measurement at low temperature (*vide supra*), corroborating the SMT behavior. The excited exchange doublet states possess much larger momenta. It is worthy to note that this complex represents the first discovery of a toroidal magnetic moment in the tetrahedron **Dy$_4$** system.

In conclusion, we reported a novel **Dy$_4$** tetrahedral complex with the Dy^{III} ions bridged by a μ_4–O center, which acts as a strong donor with short Dy–O bonds and probably produces a strong ligand field and the anisotropy axes of Dy^{III} ions pointing to the center μ_4–O. Static and dynamic magnetic investigation evidenced the small-magnetization state at low temperature and low field, as well as the behavior of the single-molecule magnet. However, *ab initio* calculations reveal that the small magnetic moment in the ground state arises

from the toroidal arrangement of the magnetic moment rather than the centripetal anisotropies. This work represents the first example of tetrahedron Dy_4 SMT, which provides a scaffold for the assembly of 3D-SMT.

We thank the Key Research Program of Frontier Sciences, CAS (ZDBS-LY-SLH023), the Key Research Program of the Chinese Academy of Sciences (ZDRW-CN-2021-3-3) and the National Natural Science Foundation of China (21871247) for financial support. J. T. gratefully acknowledges support of the Royal Society-Newton Advanced Fellowship (NA160075). L. U. acknowledges the financial support of the research projects R-143-000-A65-133 and R-143-000-A80-114 of the National University of Singapore. *Ab initio* calculations were done on the ASPIRE-1 cluster (www.nscc.sg) under the project 11001278.

Conflicts of interest

There are no conflicts to declare.

Notes and references

1 (*a*) N. Ishikawa, M. Sugita, T. Ishikawa, S.-Y. Koshihara and Y. Kaizu, *J. Am. Chem. Soc.*, 2003, **125**, 8694–8695; (*b*) L. Sorace, C. Benelli and D. Gatteschi, *Chem. Soc. Rev.*, 2011, **40**, 3092–3104; (*c*) Z. Zhu, M. Guo, X.-L. Li and J. Tang, *Coord. Chem. Rev.*, 2019, **378**, 350–364.

2 (*a*) L. Ungur and L. F. Chibotaru, *Phys. Chem. Chem. Phys.*, 2011, **13**, 20086–20090; (*b*) L. Ungur and L. F. Chibotaru, *Inorg. Chem.*, 2016, **55**, 10043–10056; (*c*) L. Norel, L. E. Darago, B. Le Guennic, K. Chakarawet, M. I. Gonzalez, J. H. Olshansky, S. Rigaut and J. R. Long, *Angew. Chem., Int. Ed.*, 2018, **57**, 1933–1938.

3 (*a*) J. Wu, J. Jung, P. Zhang, H. Zhang, J. Tang and B. Le Guennic, *Chem. Sci.*, 2016, **7**, 3632–3639; (*b*) P. Cen, M. Wang, X. Ma, L. Chen, Y.-Q. Zhang, Y. Li, D. Tian and X. Liu, *CrystEngComm*, 2020, **22**, 6856–6863; (*c*) M. Guo, J. Wu, O. Cador, J. Lu, B. Yin, B. Le Guennic and J. Tang, *Inorg. Chem.*, 2018, **57**, 4534–4542; (*d*) M. A. Sørensen, U. B. Hansen, M. Perfetti, K. S. Pedersen, E. Bartolomé, G. G. Simeoni, H. Mutka, S. Rols, M. Jeong, I. Zivkovic, M. Retuerto, A. Arauzo, J. Bartolomé, S. Piligkos, H. Weihe, L. H. Doerrer, J. van Slageren, H. M. Rønnow, K. Lefmann and J. Bendix, *Nat. Commun.*, 2018, **9**, 1292.

4 (*a*) Y.-C. Chen, J.-L. Liu, L. Ungur, J. Liu, Q.-W. Li, L.-F. Wang, Z.-P. Ni, L. F. Chibotaru, X.-M. Chen and M.-L. Tong, *J. Am. Chem. Soc.*, 2016, **138**, 2829–2837; (*b*) K.-X. Yu, J. G. C. Kragskow, Y.-S. Ding, Y.-Q. Zhai, D. Reta, N. F. Chilton and Y.-Z. Zheng, *Chem*, 2020, **6**, 1777–1793; (*c*) Y.-S. Ding, N. F. Chilton, R. E. P. Winpenny and Y.-Z. Zheng, *Angew. Chem., Int. Ed.*, 2016, **55**, 16071–16074.

5 (*a*) C. A. P. Goodwin, F. Ortu, D. Reta, N. F. Chilton and D. P. Mills, *Nature*, 2017, **548**, 439; (*b*) F.-S. Guo, B. M. Day, Y.-C. Chen, M.-L. Tong, A. Mansikkamäki and R. A. Layfield, *Science*, 2018, **362**, 1400–1403; (*c*) F. S. Guo, B. M. Day, Y. C. Chen, M. L. Tong, A. Mansikkamaki and R. A. Layfield, *Angew. Chem., Int. Ed.*, 2017, **56**, 11445–11449.

6 (*a*) J.-L. Liu, Y.-C. Chen, Y.-Z. Zheng, W.-Q. Lin, L. Ungur, W. Wernsdorfer, L. F. Chibotaru and M.-L. Tong, *Chem. Sci.*, 2013, **4**, 3310–3316; (*b*) A. Zabala-Lekuona, J. M. Seco and E. Colacio, *Coord. Chem. Rev.*, 2021, **441**, 213984; (*c*) V. S. Parmar, D. P. Mills and R. E. P. Winpenny, *Chem. – Eur. J.*, 2021, **27**, 7625–7645.

7 (*a*) H. L. C. Feltham and S. Brooker, *Coord. Chem. Rev.*, 2014, **276**, 1–33; (*b*) P. Zhang, Y.-N. Guo and J. Tang, *Coord. Chem. Rev.*, 2013, **257**, 1728–1763; (*c*) H. Wu, M. Li, Z. Xia, V. Montigaud, O. Cador, B. Le Guennic, H. Ke, W. Wang, G. Xie, S. Chen and S.-L. Gao, *Chem. Commun.*, 2020, **57**, 371–374; (*d*) J. Lu, X.-L. Li, C. Jin, Y. Yu and J. Tang, *New J. Chem.*, 2020, **44**, 994–1000; (*e*) J. Wu, Q. Yang, H. Wang, Y. Ge, J. Tang and Z. Qi, *Dalton Trans.*, 2021, **50**, 262–269.

8 (*a*) R. J. Blagg, L. Ungur, F. Tuna, J. Speak, P. Comar, D. Collison, W. Wernsdorfer, E. J. L. McInnes, L. F. Chibotaru and R. E. P. Winpenny, *Nat. Chem.*, 2013, **5**, 673–678; (*b*) J. Xiong, H.-Y. Ding, Y.-S. Meng, C. Gao, X.-J. Zhang, Z.-S. Meng, Y.-Q. Zhang, W. Shi, B.-W. Wang and S. Gao, *Chem. Sci.*, 2017, **8**, 1288–1294.

9 (*a*) X.-L. Li and J. Tang, *Dalton Trans.*, 2019, **48**, 15358–15370; (*b*) L. Ungur, S.-Y. Lin, J. Tang and L. F. Chibotaru, *Chem. Soc. Rev.*, 2014, **43**, 6894–6905.

10 (*a*) J. Tang, I. Hewitt, N. T. Madhu, G. Chastanet, W. Wernsdorfer, C. E. Anson, C. Benelli, R. Sessoli and A. K. Powell, *Angew. Chem., Int. Ed.*, 2006, **45**, 1729–1733; (*b*) J. Wu, X.-L. Li, M. Guo, L. Zhao, Y. Zhang and J. Tang, *Chem. Commun.*, 2018, **54**, 1065–1068.

11 (*a*) L. F. Chibotaru, L. Ungur and A. Soncini, *Angew. Chem., Int. Ed.*, 2008, **47**, 4126–4129; (*b*) Y.-X. Wang, W. Shi, H. Li, Y. Song, L. Fang, Y. Lan, A. K. Powell, W. Wernsdorfer, L. Ungur, L. F. Chibotaru, M. Shen and P. Cheng, *Chem. Sci.*, 2012, **3**, 3366–3370.

12 (*a*) P.-H. Guo, J.-L. Liu, Z.-M. Zhang, L. Ungur, L. F. Chibotaru, J.-D. Leng, F.-S. Guo and M.-L. Tong, *Inorg. Chem.*, 2012, **51**, 1233–1235; (*b*) J. Wu, S.-Y. Lin, S. Shen, X.-L. Li, L. Zhao, L. Zhang and J. Tang, *Dalton Trans.*, 2017, **46**, 1577–1584; (*c*) L. Zhong, W.-B. Chen, Z.-J. OuYang, M. Yang, Y.-Q. Zhang, S. Gao, M. Schulze, W. Wernsdorfer and W. Dong, *Chem. Commun.*, 2020, **56**, 2590–2593.

13 (*a*) L. Ungur, S. K. Langley, T. N. Hooper, B. Moubaraki, E. K. Brechin, K. S. Murray and L. F. Chibotaru, *J. Am. Chem. Soc.*, 2012, **134**, 18554–18557; (*b*) S.-Y. Lin, W. Wernsdorfer, L. Ungur, A. K. Powell, Y.-N. Guo, J. Tang, L. Zhao, L. F. Chibotaru and H.-J. Zhang, *Angew. Chem., Int. Ed.*, 2012, **51**, 12767–12771; (*c*) S. K. Langley, K. R. Vignesh, B. Moubaraki, G. Rajaraman and K. S. Murray, *Chem. – Eur. J.*, 2019, **25**, 4156–4165.

14 M. Perfetti, J. Rinck, G. Cucinotta, C. E. Anson, X. Gong, L. Ungur, L. Chibotaru, M.-E. Boulon, A. K. Powell and R. Sessoli, *Front Chem.*, 2019, **7**, 6.

15 G. Fernandez Garcia, D. Guettas, V. Montigaud, P. Larini, R. Sessoli, F. Totti, O. Cador, G. Pilet and B. Le Guennic, *Angew. Chem., Int. Ed.*, 2018, **57**, 17089–17093.

16 (*a*) H.-S. Wang, Q.-Q. Long, C.-L. Yin, Z.-W. Xu and Z.-Q. Pan, *Polyhedron*, 2018, **141**, 69–76; (*b*) W.-Q. Lin, X.-F. Liao, J.-H. Jia, J.-D. Leng, J.-L. Liu, F.-S. Guo and M.-L. Tong, *Chem. – Eur. J.*, 2013, **19**, 12254–12258.

17 (*a*) J. Wu, X.-L. Li, L. Zhao, M. Guo and J. Tang, *Inorg. Chem.*, 2017, **56**, 4104–4111; (*b*) L. Zhang, P. Zhang, L. Zhao, S.-Y. Lin, S. Xue, J. Tang and Z. Liu, *Eur. J. Inorg. Chem.*, 2013, 1351–1357.

18 N. F. Chilton, D. Collison, E. J. L. McInnes, R. E. P. Winpenny and A. Soncini, *Nat. Commun.*, 2013, **4**, 2551.

19 (*a*) R. Orbach, *Proc. R. Soc. London, Ser. A*, 1961, **264**, 458–484; (*b*) R. Orbach, *Proc. R. Soc. London, Ser. A*, 1961, **264**, 485–495.

20 (*a*) S. Liu, J. Lu, X.-L. Li, Z. Zhu and J. Tang, *Dalton Trans.*, 2020, **49**, 12372–12379; (*b*) M. He, F.-S. Guo, J. Tang, A. Mansikkamäki and R. Layfield, *Chem. Commun.*, 2021, **57**, 6396–6399; (*c*) X. Meng, M. Wang, X. Gou, W. Lan, K. Jia, Y.-X. Wang, Y.-Q. Zhang, W. Shi and P. Cheng, *Inorg. Chem. Front.*, 2021, **8**, 2349–2355.

21 (*a*) F. Aquilante, J. Autschbach, A. Baiardi, S. Battaglia, V. A. Borin, L. F. Chibotaru, I. Conti, L. D. Vico, M. Delcey, I. F. Galván, N. Ferré, L. Freitag, M. Garavelli, X. Gong, S. Knecht, E. D. Larsson, R. Lindh, M. Lundberg, P. Å. Malmqvist, A. Nenov, J. Norell, M. Odelius, M. Olivucci, T. B. Pedersen, L. Pedraza-González, Q. M. Phung, K. Pierloot, M. Reiher, I. Schapiro, J. Segarra-Martí, F. Segatta, L. Seijo, S. Sen, D.-C. Sergentu, C. J. Stein, L. Ungur, M. Vacher, A. Valentini and V. Veryazov, *J. Chem. Phys.*, 2020, **152**, 214117; (*b*) G. Karlström, R. Lindh, P.-Å. Malmqvist, B. O. Roos, U. Ryde, V. Veryazov, P.-O. Widmark, M. Cossi, B. Schimmelpfennig, P. Neogrady and L. Seijo, *Comput. Mater. Sci.*, 2003, **28**, 222–239; (*c*) F. Aquilante, L. De Vico, N. Ferré, G. Ghigo, P.-Å. Malmqvist, P. Neogrády, T. B. Pedersen, M. Pitoňák, M. Reiher, B. O. Roos, L. Serrano-Andrés, M. Urban, V. Veryazov and R. Lindh, *J. Comput. Chem.*, 2010, **31**, 224–247.

22 J. Wu, S. Demeshko, S. Dechert and F. Meyer, *Dalton Trans.*, 2021, **50**, 17573–17582.